POLITECNICO DI TORINO
Repository ISTITUZIONALE

Refined Finite Element Solutions for Anisotropic Laminated Plates

(Article begins on next page)

20 May 2024

Refined Finite Element Solutions for Anisotropic Laminated Plates

E. Carrera, M. Cinefra, and G. Li

Department of Mechanical and Aerospace Engineering, Politecnico di Torino,
Corso Duca degli Abruzzi 24, 10129 Torino, Italy.

Author and address for Correspondence
Dr. Erasmo Carrera
Full Professor,
Department of Mechanical and Aerospace Engineering
Politecnico di Torino,
Corso Duca degli Abruzzi, 24,
10129 Torino, ITALY,
Tel: +39 0110906836, Fax: +39 0110906899
E-mail: erasmo.carrera@polito.it

Preface

This paper is the authors tribute to this Special Issue by Composite Structures to honor Professor Yoshi Narita. It is about angle-ply laminated plates; it devotes part of the analyses to focus on the analysis geometrical boundary conditions to be used to assess finite element solutions with corresponding analytical ones. The first author would like to mention Professor Naritas attitude to 'pretend' a clear and unique definition of a given problem. Professor Narita would appreciate the discussion on geometrical boundary conditions given in the present paper.

Abstract

This paper presents some solutions for mechanical responses of angle-ply laminated plates under transverse distributed loads, which are obtained by using refined finite element models adopting variable kinematics based on Carrera's Unified Formulation (CUF). Plates with several types of stacking sequence under different boundary conditions are considered. Layer-wise (LW) models based on Chebyshev polynomials (first kind) and Equivalent Single Layer (ESL) models based on Trigonometric series are used in the analysis. To compare the performances of different displacement-based kinematic models, a set of simply supported boundary conditions and mixed clamped-free boundaries are adopted in the numerical study. A nine-node MITC (Mixed Interpolated of Tensorial Components) plate element is employed to contrast the shear locking phenomenon of thin plates. CUF-based variable kinematic models are used in the numerical study, and the numbers of expansions in thickness functions are increased until the requisite numerical accuracy are achieved, which can be conveniently implemented in the framework of CUF. By comparing the numerical results obtained with CUF-based refined models and ABAQUS 3D models as well as reference solutions from literature, the effectiveness of the adopted models is verified. The newly studied numerical cases can be taken as benchmarks for future research.

1 Introduction

Plate models are used to capture the deformation behaviors of structures of which the dimension in the thickness direction is comparatively much small than the other two in-plane dimensions. Traditional plate models such as Kirchhoff plate model (CPT, Classical Plate Theory [1]) and ReissnerMindlin theory (FSDT, First-order Shear Deformation Theory [2]) have been widely used in the analysis of laminated structures. In the last three decades, a variety of 2D models based on higher-order theories (HOT) have been proposed, as discussed by Reddy [3, 4], Palazotto and Dennis [5], et al.

Pagano [6, 7] and Srinivas [8] studied the deformation behaviors of cross-ply composite laminated plates with 3D elasticity theory. Ren [9] obtained closed-form solutions for simply supported multi-layered anisotropic plates imposed to particular types of simply-supported boundary conditions with Navier approach by expanding the external load and unknown functions into double Fourier series. This approach was also adopted by Noor [10] and Savoia [11] to obtain analytical solutions for similar cases, and the displacement field was further decomposed into a symmetric part and an anti-symmetric part in the form of double Fourier series, yet the boundary conditions they adopted seemed to be different. Savoia [11] integrated Pagano's method [6] for cross-ply laminates as a particular case. The same method was later used by Carvelli [12] and Kulikov [13, 14]. A consequence of this approach is that the transverse shear stresses σ_{xy} and σ_{yz} also consist a symmetric part and an antisymmetric part [13, 14].

Chaudhuri [15] proposed analytical solutions for angle-ply cylindrical panels and shells subjected to transverse load under SS2-type simple supports. He [16] studied the bending behaviors of rectangular antisymmetric angle-ply laminated plates under sinusoidally distributed loads with a refined deformation theory [17], which introduced additional constraints on the boundaries. Piskunov [18] developed a higher-order shear deformation theory for laminated anisotropic plates and shallow shells, in which

the boundary conditions for cross-ply and angle-ply laminates are separately defined. Similarly, to obtain Navier-type solutions, so-called SS1- and SS2-type simple supports were independently used for cross-ply and angle-ply laminated plates in some literature. Ray [19] proposed a Zeroth-Order Shear Deformation Theory and studied both symmetric and anti-symmetric laminated plates. Zuo [20] presented a wavelet finite element method adopting B-spline wavelet to investigate static and free vibration behaviors of laminated composite plates. In Nik and Tahani's work [21] that proposed analytical solutions for laminated rectangular plates with arbitrary lamination and boundary conditions by employing extended Kantorovich method, this kind of boundaries were also employed. Such definition of simple supports can be traced back to [22, 23]. Notably, Loredo [24] suggested an innovative way to define simple supports on the four edges of a plate, in which the displacements on each pair of parallel edges were coupled, and both cross-ply and angle-ply cases were addressed.

In the work of Özakça [25] on displacement-based solid finite elements for analysis of plates, two types of simple supports were adopted, namely "hard simple support" and "soft simple support" which were defined only on displacements, yet only isotropic plates were studied. Bogdanovich [26] further examined such simple supports in the investigation of laminated plates under uniformly distributed load. Kumari and Kapuria studied boundary layer effects in laminated rectangular plates using a third order zig-zag theory [27] and layer-wise theory [28], in which both "hard" and "soft" simply supported boundaries were considered. Tornabene [29] also used so-called "soft" simple supports in the static analysis of functionally graded laminated shells and panels of revolution.

Kant [30] proposed solutions on both cross-ply and angle-ply laminated plates obtained with an isoparametric finite element, in which except for on the four edges, some primary variables on the symmetry lines were also constrained. Desai [31] suggested a 3D mixed finite element model for analysis of angle-ply laminates, which treated transverse stresses $(\sigma_{xz}, \sigma_{yz}, \sigma_{zz})$ as primary nodal unknowns, and the cases of cylindrical bending, simply supported as well as clamp-clamp boundaries were considered. Chinosi [32] developed a mixed 2D model using a MITC-like approach in the framework of Reissner Mixed Variational Theorem (RMVT), with which simply supported plates with cross-ply, anti-symmetric lamination as well as plates with general stacking sequence (0°/90°) subjected to mixed edge supports (simply supported, free and clamped) were analyzed.

Carrera proposed Unified Formulation (CUF) [33, 34] as a new methodology to derive advanced plate models, which introduces thickness functions F_τ to describe the through-the-thickness kinematics of multi-layered structures. In [35] a collection of LW models and ESL models developed in the framework of CUF are summarized. Compared with classical plate theories like CLT and FSDT, CUF-based refined models have the advantage of capturing the through-the-thickness variation of transverse shear and normal stress accurately. As for finite element (FE), CUF-based refined 2D models adopting Mixed Interpolation of Tensorial Components (MITC) [36, 37] method have been successfully applied in the analysis of laminated plates to contrast the shear locking phenomenon [38, 39, 40].

CUF makes it convenient to adopt a variety of series expansion theories and interpolation polynomials to obtain FE models with variable kinematics in a compact way. Trigonometric, exponential, hyperbolic series and hierarchical Chebyshev polynomials were used to construct so-called cross-section functions for refined beam models [41, 42]. Similar applications of Legendre polynomials in the framework of CUF can be found in [43] and [44]. Various and miscellaneous thickness functions have been discussed in [39, 40].

Variable kinematics refer to the feature of CUF-based models in which the number of interpolation polynomials used in LW models or the number of series expansions employed in ESL models can be variable and determined by the particular situation to achieve requisite numerical accuracy. With a sufficient number of expansion used in the formulation, the numerical convergence can be attained, and such kinematics can be conveniently implemented in the framework of CUF without cumbersome derivation of governing equation [35]. Application of variable kinematics has been reported in [39, 40].

The primary focus of this article is the application of displacement-based refined LW models and

ESL models adopting non-Taylor series implemented in the framework of CUF in the analysis of anisotropic laminated plates under different sets of clearly stated geometrical boundary conditions (simply-supported and mixed clamped-free edges). Results obtained with ABAQUS 3D model, variable kinematic LW models adopting Chebyshev polynomials (first kind) and ESL models with trigonometric series expansion are reported and compared.

2 Geometrical and constitutive relations of multi-layered plates

In displacement-based plate theories for multi-layered structures, the in-plane strain vector ϵ_p^k and ϵ_n^k in layer k can be described by the derivatives of displacement vector $\boldsymbol{u}$ as shown in Eq. (1):

$$\epsilon_p^k = [\epsilon_{xx}^k, \epsilon_{yy}^k, \epsilon_{xy}^k]^T = \boldsymbol{D}_p \boldsymbol{u}^k, \qquad \epsilon_n^k = [\epsilon_{xz}^k, \epsilon_{yz}^k, \epsilon_{zz}^k]^T = (\boldsymbol{D}_{np} + \boldsymbol{D}_{np})\boldsymbol{u}^k \tag{1}$$

The differential operator matrices are defined as in Eq. (2):

$$\boldsymbol{D}_p = \begin{bmatrix} \partial_x & 0 & 0 \\ 0 & \partial_y & 0 \\ \partial_y & \partial_x & 0 \end{bmatrix}, \quad \boldsymbol{D}_{np} = \begin{bmatrix} 0 & 0 & \partial_x \\ 0 & 0 & \partial_y \\ 0 & 0 & 0 \end{bmatrix}, \quad \boldsymbol{D}_{nz} = \begin{bmatrix} \partial_z & 0 & 0 \\ 0 & \partial_z & 0 \\ 0 & 0 & \partial_z \end{bmatrix} \tag{2}$$

The stress-strain relations are as follows:

$$\boldsymbol{\sigma}_p^k = \boldsymbol{C}_{pp}^k \epsilon_p^k + \boldsymbol{C}_{pn}^k \epsilon_n^k, \qquad \boldsymbol{\sigma}_n^k = \boldsymbol{C}_{np}^k \epsilon_p^k + \boldsymbol{C}_{nn}^k \epsilon_n^k \tag{3}$$

in which C_{pp}^k, C_{pn}^k, C_{np}^k and C_{nn}^k are matrices of material coefficients, to be more specific:

$$\boldsymbol{C}_{pp}^k = \begin{bmatrix} C_{11}^k & C_{12}^k & C_{16}^k \\ C_{12}^k & C_{22}^k & C_{26}^k \\ C_{16}^k & C_{26}^k & C_{66}^k \end{bmatrix} \qquad \boldsymbol{C}_{pn}^k = \begin{bmatrix} 0 & 0 & C_{13}^k \\ 0 & 0 & C_{23}^k \\ 0 & 0 & C_{36}^k \end{bmatrix}$$

$$\boldsymbol{C}_{np}^k = \begin{bmatrix} 0 & 0 & 0 \\ 0 & 0 & 0 \\ C_{13}^k & C_{23}^k & C_{36}^k \end{bmatrix} \qquad \boldsymbol{C}_{nn}^k = \begin{bmatrix} C_{55}^k & C_{45}^k & 0 \\ C_{45}^k & C_{44}^k & 0 \\ 0 & 0 & C_{33}^k \end{bmatrix} \tag{4}$$

The material coefficients C_{ij} that characterize the layer material depend on the Young's moduli E_1, E_2, E_3, the shear moduli G_{12}, G_{13}, G_{23} and Poisson ratios ν_{12}, ν_{13}, ν_{23}, ν_{21}, ν_{31}, ν_{32}.

3 Variable kinematic models based on Carrera Unified Formulation

According to CUF, the displacement field $\boldsymbol{u} = \{u, v, w\}^T$ can be expressed by means of approximation functions $F_\tau(z)$ as follows in Eq. (5):

$$\begin{cases} u(x,y,z) = F_0(z)u_0(x,y) & +F_1(z)u_1(x,y) & +\cdots+F_N(z)u_N(x,y) \\ v(x,y,z) = F_0(z)v_0(x,y) & +F_1(z)v_1(x,y) & +\cdots+F_N(z)v_N(x,y) \\ w(x,y,z) = F_0(z)w_0(x,y) & +F_1(z)w_1(x,y) & +\cdots+F_N(z)w_N(x,y) \end{cases} \tag{5}$$

In a more compact form, CUF can be expressed as shown in Eq. (6) for ESL models and in Eq. (7) for LW models respectively:

$$\boldsymbol{u}(x,y,z) = F_\tau(z)\boldsymbol{u}_\tau(x,y); \qquad \delta\boldsymbol{u}(x,y,z) = F_s(z)\delta\boldsymbol{u}_s(x,y) \qquad \tau, s = 0, 1, ..., N \tag{6}$$

$$\boldsymbol{u}^k(x,y,\zeta_k) = F_\tau^k(\zeta_k)\boldsymbol{u}_\tau(x,y); \qquad \delta\boldsymbol{u}^k(x,y,\zeta_k) = F_s^k(\zeta_k)\delta\boldsymbol{u}_s(x,y) \qquad \tau, s = 0, 1, ..., N \tag{7}$$

$\delta \boldsymbol{u}$ indicates the virtual displacement associated with the virtual work when Principle of Virtual Displacement (PVD) is applied and k is the layer index in laminated plates. $F_\tau^{(k)}$ and $F_s^{(k)}$ are the approximation functions, which are also named as thickness functions since they are defined in the thickness domain $z \in [-\frac{h}{2}, \frac{h}{2}]$ for ESL models or $\zeta_k \in [-1, 1]$ for LW models. Note that F_τ and F_τ^k are independently employed in annotation, which implies that differently from ESL models, in LW models primary variables are allocated to each layer. N is the order of interpolation polynomials (for LW) or number of series expansion (except the constant term, for ESL) adopted in the thickness direction. $\boldsymbol{u}_\tau^{(k)}(x, y)$ and $\boldsymbol{u}_s^{(k)}(x, y)$ represent the unknown primary variables which are the coefficients corresponding to expansion terms $F_\tau^{(k)}$ and $F_s^{(k)}$, respectively. τ and s are Einstein's summation subscripts.

CUF can describe many existing deformation theories. When $F_s(z)$ and $F_\tau(z)$ are defined in the whole through-the-thickness domain using ESL model, by substituting $F_\tau = z^\tau (\tau = 0, 1, \cdots, N)$ as shown in Eq. (8), one obtains Higher-Order Deformation Theory. FSDT [2] can be obtained with an ESL approach with $N = 1$, by imposing a constant transverse displacement through the thickness via penalty method. CPT [1] can be expressed by employing a penalty technique to the constitutive equations to enforce that the transverse shear strains are null when written in CUF.

$$F_0 = z^0 = 1, \quad F_1 = z^1 = z, \quad \ldots, \quad F_N = z^N \tag{8}$$

Alternatively, if F_τ^k represents Lagrange interpolation polynomials defined in each layer thickness domain $\zeta_k \in [-1, 1]$, as shown in Eq. (9), CUF will lead to a LW model based on Lagrange polynomials. ζ_{k_τ} are located at the prescribed interpolation nodes. $\zeta_{k_0} = -1$ and $\zeta_{k_N} = 1$ correspond to the bottom and top surfaces of the kth layer, respectively.

$$F_\tau^k(\zeta_k) = \prod_{i=0, i \neq s}^{N} \frac{\zeta_k - \zeta_{k_i}}{\zeta_{k_\tau} - \zeta_{k_i}} \tag{9}$$

CUF provides a convenient approach in implementing different series expansion theories and interpolation approximation methods in a unified manner to obtain refined 2D kinematics for multi-layered structures.

3.1 Refined ESL models based on Trigonometric series

In the framework of ESL models, if trigonometric sine series together with a constant term are adopted, the displacement vector can be written as follows in Eq. (10):

$$\boldsymbol{u}(x, y, z) = \boldsymbol{u}_0(x, y) + \sin\left(\frac{\pi z}{h}\right) \boldsymbol{u}_1(x, y) + \ldots + \sin\left(\frac{n\pi z}{h}\right) \boldsymbol{u}_N(x, y) \tag{10}$$

where h is the thickness of the laminated plate and n is the number of half-waves. Accordingly, a similar description can be obtained using trigonometric cosine series:

$$\boldsymbol{u}(x, y, z) = \boldsymbol{u}_0(x, y) + \cos\left(\frac{\pi z}{h}\right) \boldsymbol{u}_1(x, y) + \ldots + \cos\left(\frac{n\pi z}{h}\right) \boldsymbol{u}_N(x, y) \tag{11}$$

A model adopting full trigonometric series becomes Eq. (12) when $N = 2n$:

$$\boldsymbol{u}(x, y, z) = \boldsymbol{u}_0(x, y) + \sin\left(\frac{\pi z}{h}\right) \boldsymbol{u}_1(x, y) + \cos\left(\frac{\pi z}{h}\right) \boldsymbol{u}_2(x, y) + \ldots + \sin\left(\frac{n\pi z}{h}\right) \boldsymbol{u}_{N-1}(x, y) + \\ + \cos\left(\frac{n\pi z}{h}\right) \boldsymbol{u}_N(x, y) \tag{12}$$

or Eq. (13) when $N = 2n + 1$:

$$\boldsymbol{u}(x,y,z) = \boldsymbol{u}_0(x,y) + \sin\left(\frac{\pi z}{h}\right)\boldsymbol{u}_1(x,y) + \cos\left(\frac{\pi z}{h}\right)\boldsymbol{u}_2(x,y) + ... + \cos\left(\frac{n\pi z}{h}\right)\boldsymbol{u}_{N-1}(x,y) +$$
$$+ \sin\left(\frac{(n+1)\pi z}{h}\right)\boldsymbol{u}_N(x,y) \tag{13}$$

Since pure sine series apply to approximate odd functions, while cosine series suit even functions, full trigonometric series expansions Eq. (12) and Eq. (13) are recommended for more general cases, which are adopted in the following numerical study.

3.2 Refined ESL models with Murakami zig-zag function

Because of the intrinsic anisotropy of multi-layered structures, the first order derivative of the displacement variables through the thickness is discontinuous. Fortunately, with ESL models, it is possible to capture the zig-zag effects by employing the Murakami theory [45]. A zig-zag term can be introduced into Equation (6), leading to so-called zig-zag models as shown in Eq. (14):

$$\boldsymbol{u} = F_0\,\boldsymbol{u}_0\ +\ ...\ +\ F_N\,\boldsymbol{u}_N\ +\ (-1)^k\zeta_k\boldsymbol{u}_Z. \tag{14}$$

In Eq. (14) subscript Z refers to the introduced zig-zag term. Refined theories can be obtained by adding the zig-zag term to the Taylor polynomials expansion, trigonometric or other types of series expansion.

3.3 Refined LW models based on Chebyshev polynomials

The continuity of transverse stresses at layer interfaces can be satisfied naturally when LW models with a sufficient number of expansion terms are adopted, which has been demonstrated in the authors' previous work [40]. According to LW models, the displacement defined in the domain of layer k can be expressed as shown in Eq. (15):

$$\boldsymbol{u}^k =\ F_b\,\boldsymbol{u}_b^k\ +\ F_t\,\boldsymbol{u}_t^k\ +\ F_r\,\boldsymbol{u}_r^k\ =\ F_\tau\,\boldsymbol{u}_\tau^k \qquad \tau = t,b,r; \quad r = 2,...,N. \tag{15}$$

The expression of the expansions can be derived from Eq. (16):

$$F_b = \frac{T_0 - T_1}{2}, \quad F_t = \frac{T_0 + T_1}{2}, \quad F_r = T_r - T_{r-2}. \tag{16}$$

in which $T_j(\zeta_k)$ employs Chebyshev polynomials (first kind) to the jth order defined in the isoparametric domain within layer k: $-1 \leq \zeta_k \leq 1$. The displacements on bottom (b) and top (t) surface of layer k are used as unknown variables and following compatibility conditions are imposed to the formulations:

$$u_t^k = u_b^{k+1}, \quad k = 1, N_l - 1. \tag{17}$$

where N_l represents the total number of layers in a laminated plate.

4 FE discretization and governing equations

This section presents the derivation of the governing equations for CUF-based refined finite element models according to the PVD (Principle of Virtual Displacement) in the case of multi-layered plates.
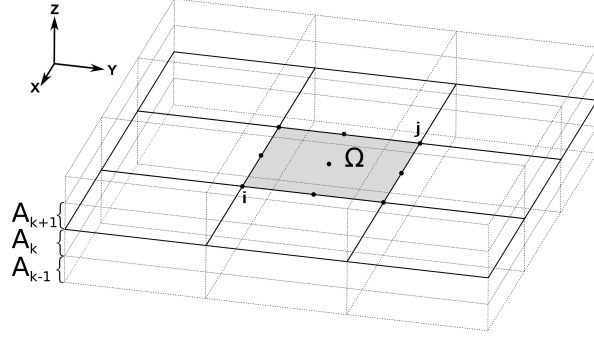
Figure 1: 3D field discretization with CUF-based advanced plate FE models.

Fig. 1 illustrates the 3D filed discretization with CUF-based refined plate models, which can approximate 3D displacement field and capture spatial stress distribution. Ω represents the in-plane domain of an element el, and A_k indicates the through-the-thickness domain corresponding to layer k.

For a nine-node plate element, the displacement vector interpolated on the element nodes using Lagrangian shape functions N_i and N_j reads:

$$\boldsymbol{u}_\tau(x,y) = N_i(x,y)\boldsymbol{U}_{i\tau}, \qquad \delta\boldsymbol{u}_s(x,y) = N_j(x,y)\delta\boldsymbol{U}_{js} \qquad i,j = 1,\cdots,9 \tag{18}$$

where $\delta\boldsymbol{U}_{i\tau}$ and $\boldsymbol{U}_{sj}$ are the vector of generalized nodal displacements (constant weighting coefficients) and its virtual variation, respectively. Utilizing CUF-based, the displacement field in the domain defined by element le and layer k can be expressed as shown in Eq. (19) for ESL models, in which $z \in [z_{bottom}, z_{top}]$:

$$\begin{aligned}
\boldsymbol{u}^k(x,y,z) &= N_i(x,y)F_\tau(z)\boldsymbol{U}_{i\tau} & i &= 1,\cdots,9; & \tau &= 1,\cdots,N \\
\delta\boldsymbol{u}^k(x,y,z) &= N_j(x,y)F_s(z)\boldsymbol{U}_{js} & j &= 1,\cdots,9; & s &= 1,\cdots,N
\end{aligned} \tag{19}$$

and in Eq. (20) for LW models, in which $\zeta_k \in [-1,1]$:

$$\begin{aligned}
\boldsymbol{u}^k(x,y,\zeta_k) &= N_i(x,y)F_\tau^k(\zeta_k)\boldsymbol{U}_{i\tau}^k & i &= 1,\cdots,9; & \tau &= 1,\cdots,N \\
\delta\boldsymbol{u}^k(x,y,\zeta_k) &= N_j(x,y)F_s^k(\zeta_k)\boldsymbol{U}_{js}^k & j &= 1,\cdots,9; & s &= 1,\cdots,N
\end{aligned} \tag{20}$$

The superscript k of $\boldsymbol{U}_{i\tau}^k$ implies that in LW FE models each layer possesses independent degrees of freedom. In a compact form, the strain expression Eq. (1) will become as shown in Eq. (21):

$$\begin{cases}
\boldsymbol{\epsilon}_p^k = F_\tau^{(k)}\boldsymbol{D}_p(N_i\boldsymbol{I})\boldsymbol{U}_{i\tau}^{(k)} \\
\boldsymbol{\epsilon}_n^k = F_\tau^{(k)}\boldsymbol{D}_{np}(N_i\boldsymbol{I})\boldsymbol{U}_{i\tau}^{(k)} + F_{\tau,z}^{(k)}N_i\boldsymbol{I}\boldsymbol{U}_{i\tau}^{(k)}
\end{cases} \tag{21}$$

in which $\boldsymbol{I}$ is a 3×3 identity matrix. A MITC9 plate element is formulated by using a specific interpolation strategy to derive the strain components on a nine-node element, and the corresponding interpolation points are known as *tying points*, which are as illustrated in Fig. 2. Note that the normal strain component in the third direction ϵ_{zz} is derived directly from the displacement expression.

The Lagrangian interpolating functions are arranged as follows Eq. (22):

$$\begin{cases}
N_{m1} = [N_{A1}, N_{B1}, N_{C1}, N_{D1}, N_{E1}, N_{F1}], \\
N_{m2} = [N_{A2}, N_{B2}, N_{C2}, N_{D2}, N_{E2}, N_{F2}], \\
N_{m3} = [N_P, N_Q, N_R, N_S].
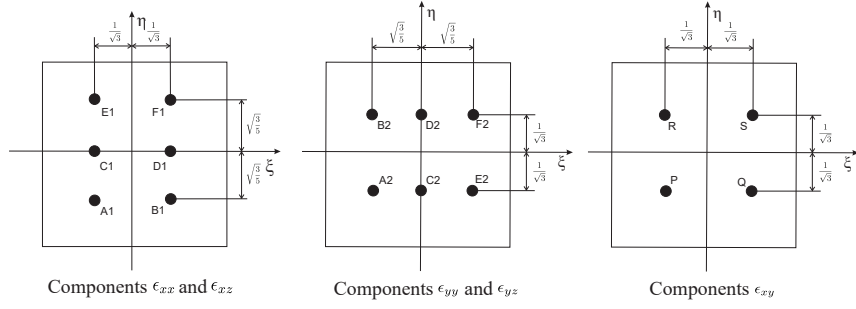\end{cases} \tag{22}$$

7

Figure 2: Tying points on a MITC9 plate element.

where the subscripts m1, m2 and m3 indicate the point groups (A1,B1,C1,D1,E1,F1), (A2,B2,C2,D2,E2,F2) and (P,Q,R,S), respectively. Accordingly, the strain components can be expressed as follows:

$$
\begin{cases}
\boldsymbol{\epsilon}_p^{(k)} = \begin{bmatrix} \epsilon_{xx}^{(k)} \\ \epsilon_{yy}^{(k)} \\ \epsilon_{xy}^{(k)} \end{bmatrix} = \begin{bmatrix} N_{m1} & 0 & 0 \\ 0 & N_{m2} & 0 \\ 0 & 0 & N_{m3} \end{bmatrix} \begin{bmatrix} \epsilon_{xx_{m1}}^{(k)} \\ \epsilon_{yy_{m2}}^{(k)} \\ \epsilon_{xy_{m3}}^{(k)} \end{bmatrix}, \\[30pt]
\boldsymbol{\epsilon}_n^{(k)} = \begin{bmatrix} \epsilon_{xz}^{(k)} \\ \epsilon_{yz}^{(k)} \\ \epsilon_{zz}^{(k)} \end{bmatrix} = \begin{bmatrix} N_{m1} & 0 & 0 \\ 0 & N_{m2} & 0 \\ 0 & 0 & 1 \end{bmatrix} \begin{bmatrix} \epsilon_{xz_{m1}}^{(k)} \\ \epsilon_{yz_{m2}}^{(k)} \\ \epsilon_{zz_{m3}}^{(k)} \end{bmatrix}.
\end{cases}
\tag{23}
$$

in which strains $\epsilon_{xx_{m1}}$, $\epsilon_{yy_{m2}}$, $\epsilon_{xy_{m3}}$, $\epsilon_{xz_{m1}}$ and $\epsilon_{yz_{m2}}$ are derived from Eq. (21) and the shape functions N_i and corresponding derivatives are evaluated on the tying points.

Considering a basic spatial domain identified by element el and layer k, taking into account the constitutive equations Eq. (3), the strain expression in the form of MITC method Eq. (23) as well as CUF-type FE displacement expression Eq. (19) or Eq. (20) discussed above, by applying PVD, one can obtain the expression of internal work as:

$$
\delta L_{int} = \int_\Omega \int_{A_k} (\delta \boldsymbol{\epsilon}_n^{k\,T} \boldsymbol{\sigma}_n^k + \delta \boldsymbol{\epsilon}_p^{k\,T} \boldsymbol{\sigma}_p^k) dA_k d\Omega = \delta \boldsymbol{U}_{js}^{(k)\,T} \boldsymbol{K}_{js\tau i}^k \boldsymbol{U}_{i\tau}^{(k)}
\tag{24}
$$

where $\boldsymbol{K}_{js\tau i}^k$ is the stiffness matrix. A generic surface load acting on a horizontal surface of the plate can be denoted as $p_\alpha(x, y)$, where the subscript α indicates the direction of the load, which can equal to x, y or z. The virtual variation of the external work caused by p_α can be expressed as Eq. (25):

$$
\delta L_{ext}^{p_\alpha} = \int_\Omega \delta u_\alpha^{(k)} p_\alpha d\Omega = \int_\Omega \delta u_{\alpha_{sj}}^{(k)} N_j F_s^{(k)}(z_p) p_\alpha d\Omega
\tag{25}
$$

in which z_p represents the coordinate of the loading surface. If the external surface load is written into a vector as $\boldsymbol{p}_\alpha(x, y)$ ($[p_x, 0, 0]^T$, $[0, p_y, 0]^T$ or $[0, 0, p_z]^T$), Eq. (25) can be further expressed in a vector form as in Eq. (26), where $\boldsymbol{P}_{js}^k$ is the FE load vector expression in which only the components on α direction are non-zero.

$$
\delta L_{ext}^{p_\alpha} = \delta \boldsymbol{U}_{js}^{(k)\,T} \boldsymbol{P}_{js}^{(k)}
\tag{26}
$$

Thus the governing equation can be expressed as Eq. (27):

$$
\delta \boldsymbol{U}_{js}^{(k)\,T} : \quad \boldsymbol{K}_{js\tau i}^{(k)} \boldsymbol{U}_{i\tau}^{(k)} = \boldsymbol{P}_{js}^{(k)}
\tag{27}
$$

The 3×3 matrix $\boldsymbol{K}_{js\tau i}^k$ is the so-called fundamental nucleus of stiffness in the context of CUF, which is the core unit of the element stiffness matrix. By adopting the Einstein summation convention, the

8

stiffness matrix of the spatial domain identified by Ω and k can be obtained. $\boldsymbol{P}_{js}^{(k)}$ is the fundamental nucleus of external load. For more details about the derivation, one can refer to [35] and [38].

For multi-layered structures, in the case of LW models, by assembling the stiffness matrices corresponding to each layer and overlapping the components at layer interfaces, the complete nodal stiffness matrix of an element can be acquired, and for ESL models the stiffness matrices from different layers will be lumped together.

5 Numerical study

5.1 Setting of boundary conditions

Generally speaking, the edge supports can be imposed on the displacements, stresses, boundary moments and forces, and the boundary condition setting is directly related to the formulations adopted. Historically, the simple supports for plates and shells have been classified into two types, namely SS1 and SS2 [4, 22, 23]. Based on the Navier approach, SS2 have been successfully used in the analysis of cross-ply laminated plates [6]. While for angle-ply laminates, there have been some arguments. Adoption of SS1 for angle-ply laminates while SS2 for cross-ply problems are reported in [18, 19, 20, 21]. Whereas such definitions differentiate cross-ply laminates from angle-ply anisotropic laminates, which are more mathematically meaningful to apply Navier's approach rather than physically meaningful. Also, such definitions are only applicable to a specific set of cases. Especially, Sovia's [11] variational approach used two sets of displacement variables, and boundary conditions of each set need to be satisfied separately, however considering transverse shear stresses σ_{xz} or σ_{yz} at the center of edges, only the results correspond to either the symmetric part or antisymmetric part was reported. As for models based on Mixed Variational Theorem, not only boundary displacements need to be defined, the additional primary variables (transverse shear stresses σ_{xz} and σ_{yz}, for example) should also be addressed.

Apparently, all the above-described boundary conditions used in most published articles for simply supported angle-ply laminates have met difficulties when applied to displacement-based finite element models such as 3D brick elements, 2D LW models, and non-Taylor based ESL models. To take the advantage of such models in obtaining numerical solutions for general angle-ply laminated plate, suitable boundary conditions are necessary and should be explicitly specified by stating.

Jones described four kinds of simply-supported boundary conditions in [46], as shown in Fig. 3, among which S4 refers to boundary conditions that permit translation in any direction in the x-y plane. If S4 is taken as a reference, to avoid stress concentration, geometrical constraints can be set on the edge surfaces rather than the edge of the middle surface, and the boundary value of bending moments and forces of S4 can still be satisfied (such as $M_x = N_x = N_{xy}$ on edge $x = 0$). Such simple supports are easy to be applied on displacement-based 3D models, refined 2D LW models and non-Taylor based ESL models. To be more specific, the simply supported and clamped boundary conditions adopted in the following sections are as shown in Table 1, in which the subscript τ is the expansion index, and superscript k is the layer index.

Table 1: Definition of displacement boundary conditions on geometrical edges

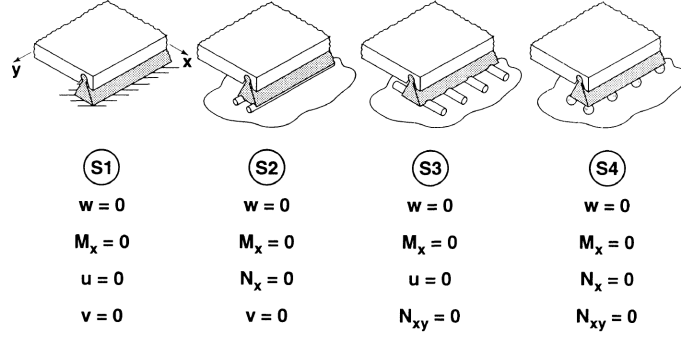| Boundary types	3D brick element	CUF-based plate models	
		ESL	LW
Simply supported	$w = 0$	$w_\tau = 0$	$w_\tau^k = 0$
Clamped	$u = v = w = 0$	$u_\tau = v_\tau = w_\tau = 0$	$u_\tau^k = v_\tau^k = w_\tau^k = 0$

9

Figure 3: Simply supported edge boundary conditions for a plate, Figure D-8 in Jones [46].

Note that when the simple supports in Table 1 are enforced to all the four edges of a plate, three in-plane rigid body motion modes still exist: two translation mode and one rotation mode. To eliminate rigid body motion modes, small penalty stiffness needs to be introduced to at least two nodes on both x and y directions, and the penalty value should be small enough to avoid influencing the stress field but large enough to constrain the unnecessary displacements. In ABAQUS, this can be easily implemented with spring elements that connect the two nodes to "the ground".

5.2 Acronyms

An acronym system is given here to denote the related kinematics. For LW models, LW-CBTn denotes a model adopting Chebyshev polynomials of the first kind to the nth order, which includes $n + 1$ expansions in total. ESL models adopting full trigonometric series including both sine and cosine terms are indicated by ESL-TRGn, in which the final number n represents the number of expansion terms used in the thickness functions F_τ except the constant term. If a letter Z follows an ESL acronym, a Murakami zig-zag term will be added to the displacement functions. Taking ESL-TRG3Z as an example, it refers to the following kinematics:

$$\boldsymbol{u}(x,y,z) = \boldsymbol{u}_0(x,y) + \sin(\frac{\pi z}{h})\boldsymbol{u}_1(x,y) + \cos(\frac{\pi z}{h})\boldsymbol{u}_2(x,y) + \sin(\frac{2\pi z}{h})\boldsymbol{u}_3(x,y) + (-1)^k \zeta_k \boldsymbol{u}_{4_Z} \qquad (28)$$

5.3 Numerical cases

Numerical study of several cases is reported in this section. The attention is restricted to square angle-ply plates subjected to distributed loads under simply supported boundary conditions and mixed clamped-free boundary conditions as have been stated in Table 1. For all the cases studied, the orthotropic layer material coefficients are listed as follows referring to Savoia and Reddy [11]:

$$E_L = 25 \text{ psi (176 GPa)}, \quad E_T = 10^6 \text{ psi (7 GPa)}, \quad G_{LT} = 0.510^6 \text{ psi (3.5 GPa)},$$
$$G_{TT} = 0.2 \text{ psi (1.4 GPa)}, \quad \nu_{LT} = \nu_{TT} = 0.25. \qquad (29)$$

where E, G and ν denotes the Young's modulus, shear modulus, and Poisson's ratio, respectively. L indicates fiber longitudinal and T transverse direction. To compare the results, the following non-dimensionalization parameters are used:

$$\bar{w} = 100w\frac{E_T h^3}{p_0 a^4}, \quad \{\bar{\sigma}_{xx}, \bar{\sigma}_{yy}, \bar{\sigma}_{xy}\} = \{\sigma_{xy}, \sigma_{yy}, \sigma_{xy}\}\frac{h^2}{p_0 a^2},$$
$$\{\bar{\tau}_{xz}, \bar{\tau}_{yz}\} = \{\tau_{xz}, \tau_{yz}\}\frac{h}{p_0 a}, \quad \bar{\sigma}_{zz} = \sigma_{zz}/p_0, \quad \bar{z} = z/h. \qquad (30)$$

10

Only square plates are analyzed in the following numerical cases, and $a = b = 1$ is adopted. All the plates analyzed have layers of equal thickness. An amplitude of the distributed load $p_0 = 1$ is used. The stacking sequence is described from bottom to top by default.

5.3.1 Simply-supported thick square plates with $(-15°/15°)$ and $(-30°/30°/ - 30°/ - 30°)$

Simply supported antisymmetric angle-ply laminated plates subjected to bi-sinusoidally distributed load on both top and bottom surfaces are studied. The analyzed plates are:

- $(-15°/15°)$ plate with span-to-thickness ratio $a/h = 4$;

- $(-30°/30°/ - 30°/30°)$ plate with span-to-thickness ratio $a/h = 10$.

The subjected transverse loads as shown in Eq. (31) are imposed to the square plates:

$$p_t(x, y) = -\frac{p_0}{2} \sin \frac{\pi x}{a} \sin \frac{\pi y}{b}, \quad p_b(x, y) = -\frac{p_0}{2} \sin \frac{\pi x}{a} \sin \frac{\pi y}{b} \tag{31}$$

in which p_t and p_b refer to the load on the top and bottom surface, respectively, and their negative sign implies the loading direction.

The results are compared with the reference solutions proposed by Savoia [11]. Note that Savoia [11] used two set of coordinate functions and each set has its specific boundary conditions, which is different from the simple supports used in this case as shown in Table 1.

For angle-ply laminated plates, symmetry on the center lines no longer exists, so the whole plate should be modeled. ABAQUS 3D brick element C3D20R (20-node quadratic brick element with reduced integration), plate models LW-CBTn and ESL-TRGnZ are adopted in the analysis. With the increase of the number of expansion terms, numerically converged displacement and stresses can be acquired with requisite accuracy. By using a relative error threshold of 2%, for the two-layered plate LW-CBT5 and ESL-TRG9Z can achieve the convergence, and for the four-layered plate with $a/h = 10$ LW-CBT4 and ESL-TRG11Z are sufficient to guarantee the numerical convergence. At the same time, to achieve convergence related to element size, FE mesh grids of 10×10 and 16×16 are adopted for the two-layered and four-layered plates, respectively. Meanwhile, ABAQUS models used eight brick elements through the thickness of each layer, and the elements have an aspect ratio (in-plane dimension over thickness) of 6.4 for two-layered and 20 for four-layered plates, respectively.

Fig. 4 and Fig. 5 summarize the stress variation through the thickness at $(\frac{a}{2}, \frac{b}{2})$ and $(\frac{a}{2}, 0)$. The results show that CUF-based refined models are capable of capturing the 3D stress distribution over the laminated plates in detail. Solutions attained with variable kinematics including LW-CBTn and ESL-TRGnZ show good agreement with ABAQUS 3D results for the two thick plates studied. Because of the difference in boundary conditions, the FE models adopted provide different results from Savoia's analytical solutions [11], but with very similar through-the-thickness variation. It should be noted that for the plate with four layers, comparatively speaking, LW-CBTn have better performance than ESL-TRGnZ considering the through-the-thickness variation of transverse shear stress. By the way, possibly the signs of $\bar{\sigma}_{xy}$ and $\bar{\sigma}_{yz}$ are inverted in [11].

(a) $a/h = 4$, $\bar{\sigma}_{xx}\left(\frac{a}{2}, \frac{b}{2}, \bar{z}\right)$

(b) $a/h = 4$, $\bar{\sigma}_{xy}\left(\frac{a}{2}, \frac{b}{2}, \bar{z}\right)$

(c) $a/h = 4$, $\bar{\sigma}_{xz}\left(\frac{a}{2}, 0, \bar{z}\right)$

(d) $a/h = 4$, $\bar{\sigma}_{yz}\left(\frac{a}{2}, 0, \bar{z}\right)$

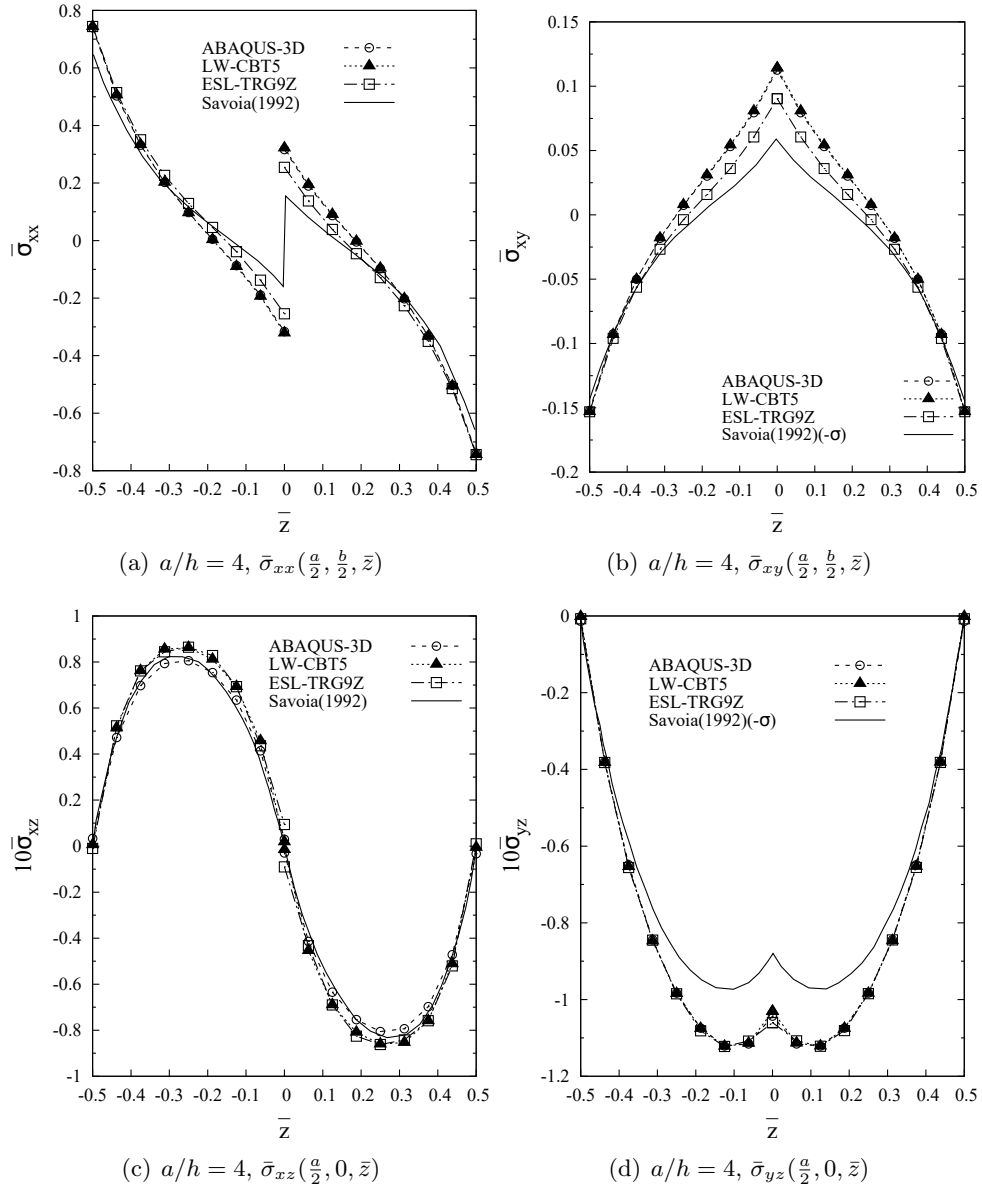Figure 4: Stress variation through the thickness, simply supported square plate with $(-15°/15°)$, subjected to bi-sinusoidally distributed load on both top and bottom surfaces, $a/h = 4$.

(a) $a/h = 10$, $\bar{\sigma}_{xx}\left(\frac{a}{2}, \frac{b}{2}, \bar{z}\right)$

(b) $a/h = 10$, $\bar{\sigma}_{xy}\left(\frac{a}{2}, \frac{b}{2}, \bar{z}\right)$

(c) $a/h = 10$, $\bar{\sigma}_{xz}\left(\frac{a}{2}, 0, \bar{z}\right)$
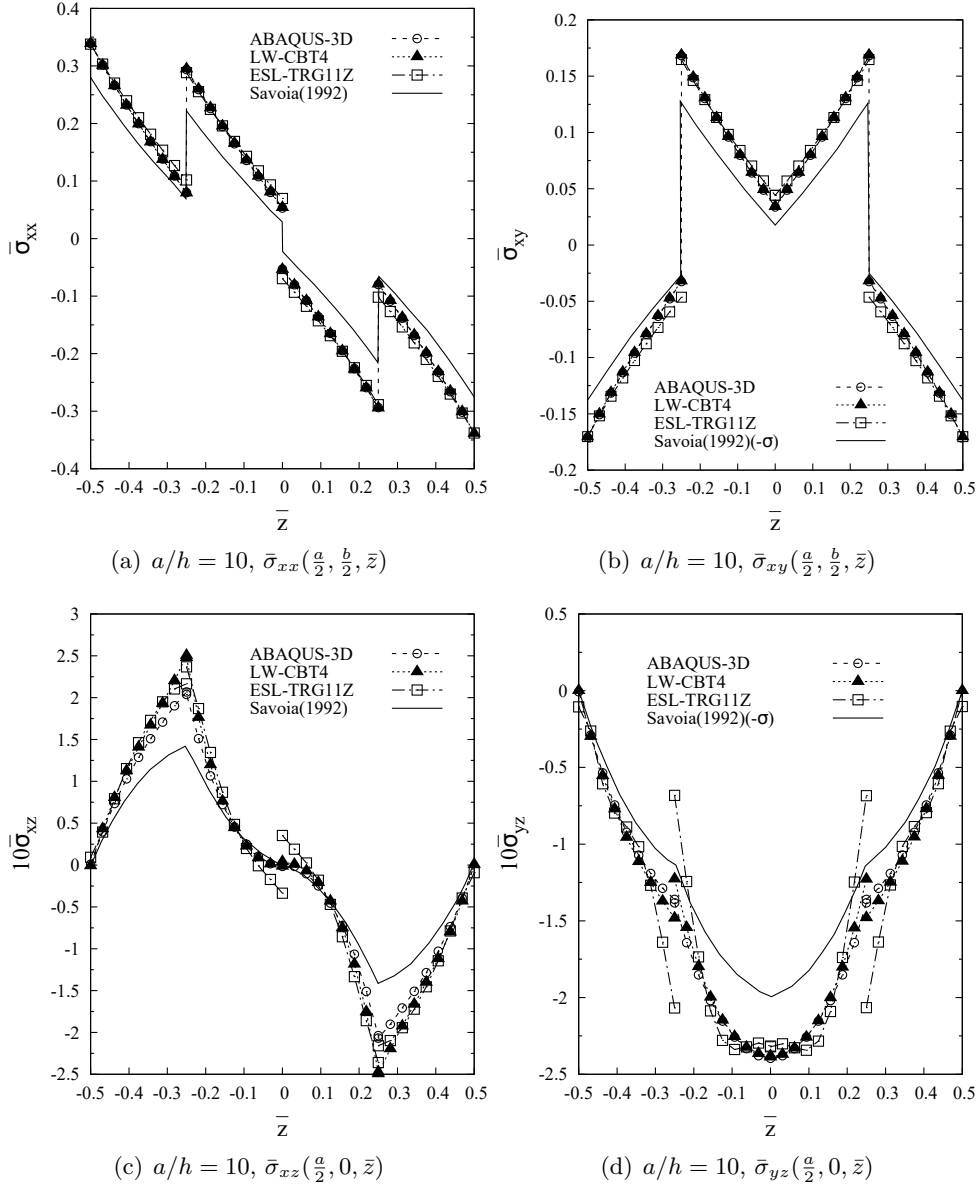
(d) $a/h = 10$, $\bar{\sigma}_{yz}\left(\frac{a}{2}, 0, \bar{z}\right)$

Figure 5: Stress variation through the thickness, simply supported square plate with $(-30°/30°/-30°/30°)$, subjected to bi-sinusoidally distributed load on both top and bottom surfaces, $a/h = 10$.

5.3.2 Simply supported square thick and thin plates with $(0°/30°)$

This numerical case considers a two-layered square plate with a general lamination of $(0°/30°)$ subjected to bi-sinusoidally distributed pressure on its top and bottom surfaces, under simply supported boundary conditions. The load adopted is as shown in Eq. (31).

Variable kinematic model LW-CBTn and ESL-TRGnZ are used in analysis, and results obtained by above-mentioned ABAQUS 3D model are also listed for comparison. Both mesh grid convergence and expansion convergence have been reported in Table 2. For the case of $a/h = 4$, the maximum relative error is less than 1.5%; meanwhile for $a/h = 50$, this value is 3% except the case of $\bar{\sigma}_{zz}$. Note that the ABAQUS 3D model used for the thin plate ($a/h = 50$) has an in-plane mesh of 80×80, which means the brick elements have an aspect ratio of 10. It can be found that results obtained with CUF-based refined models are in good agreement with ABAQUS 3D results.

13

Fig. 6 shows the through-the-thickness variation of stresses on two in-plane points of the plate. Fig. 7 and Fig. 8 illustrate the contour plots of σ_{yz} of two-layered plate with $a/h = 4$ and $a/h = 50$, respectively, in which it can be found that when the plate becomes thin, the stress distribution becomes very different from the case of thick plate and the maximum stress location moves to the edge corners.

Results in Table 2, Figs. 6 to 8 show that CUF-based refined models with variable kinematics LW-CBTn and ESL-TRGnZ are less sensitive to the aspect ratio of laminated plates, which can obtain solutions with comparable accuracy but less computational costs compared with 3D models, especially for thin structures. Moreover, CUF-based plate models support any arbitrary number of output points through the thickness in post-processing, while for a model with brick elements the number of output nodes depends on the number of element used explicitly, and the stresses on these nodes are extrapolated from the integration points.

Table 2: Displacement and stress evaluation of square plate with (0°/30°) subjected to simply-supported boundary conditions.

a/h	Kinematics	Mesh	$\bar{w}$ $(\frac{a}{2}, \frac{b}{2}, 0)$	$\bar{\sigma}_{xx}$ $(\frac{a}{2}, \frac{b}{2}, \frac{-h}{2})$	$\bar{\sigma}_{yy}$ $(\frac{a}{2}, \frac{b}{2}, \frac{h}{2})$	$\bar{\sigma}_{xy}$ $(\frac{a}{2}, \frac{b}{2}, \frac{h}{2})$	$10\bar{\sigma}_{xz}$ $(\frac{a}{2}, 0, \frac{h}{4})$	$10\bar{\sigma}_{yz}$ $(\frac{a}{2}, 0, \frac{h}{4})$	$\bar{\sigma}_{zz}$ $(\frac{a}{2}, \frac{b}{2}, \frac{-h}{2})$	DOFs
	LW-CBT4	8×8	-1.956	0.8171	-0.2299	-0.2561	-1.543	-1.483	0.5036	6069
	LW-CBT4	10×10	-1.957	0.8138	-0.2301	-0.2568	-1.534	-1.475	0.5032	9261
	LW-CBT5	10×10	-1.957	0.8139	-0.2301	-0.2569	-1.487	-1.453	0.5012	11907
4	LW-CBT6	10×10	-1.957	0.8139	-0.2301	-0.2569	-1.487	-1.453	0.5004	14553
	ESL-TRG7Z	10×10	-1.957	0.8131	-0.2299	-0.2566	-1.546	-1.486	0.5036	11907
	ESL-TRG9Z	10×10	-1.958	0.8139	-0.2301	-0.2569	-1.498	-1.458	0.5052	14553
	ESL-TRG11Z	10×10	-1.958	0.8138	-0.2300	-0.2569	-1.482	-1.450	0.4984	17199
	ABAQUS-3D	10×10	-1.941	0.8067	-0.2298	-0.2571	-1.451	-1.449	0.5017	23199
	LW-CBT3	18×18	-0.7833	0.6175	-0.1578	-0.1937	-8.897	-3.256	0.5410	20535
	LW-CBT3	20×20	-0.7836	0.6174	-0.1579	-0.1939	-9.093	-3.287	0.5430	25215
	LW-CBT4	20×20	-0.7836	0.6174	-0.1579	-0.1939	-9.091	-3.286	0.5010	35301
50	ESL-TRG11Z	20×20	-0.7836	0.6173	-0.1579	-0.1939	-9.026	-3.147	0.5635	65559
	ESL-TRG13Z	20×20	-0.7836	0.6174	-0.1579	-0.1939	-9.000	-3.240	0.5070	75645
	ABAQUS-3D	50×50	-0.7846	0.6170	-0.1581	-0.1944	-8.719	-2.981	0.5025	517599
	ABAQUS-3D	80×80	-0.7848	0.6169	-0.1581	-0.1944	-9.154	-3.036	0.5025	1310499

(a) $\bar{\sigma}_{xx}\left(\frac{a}{2}, \frac{b}{2}, \bar{z}\right)$

(b) $\bar{\sigma}_{xy}\left(\frac{a}{2}, \frac{b}{2}, \bar{z}\right)$

(c) $\bar{\sigma}_{xz}\left(\frac{a}{2}, 0, \bar{z}\right)$

(d) $\bar{\sigma}_{yz}\left(\frac{a}{2}, 0, \bar{z}\right)$
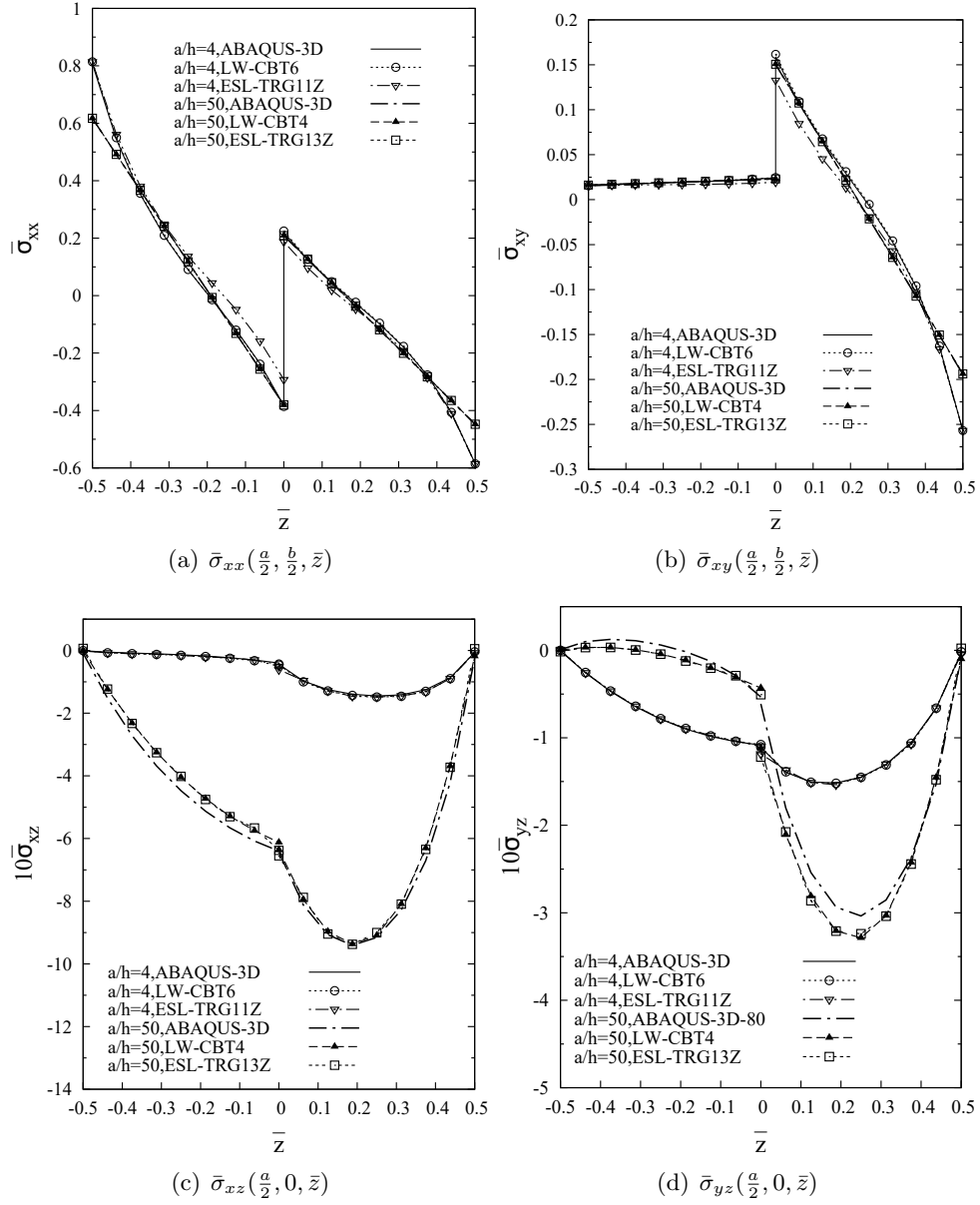
Figure 6: Through-the-thickness variation of stresses, simply supported square plate with$(0°/30°)$, subjected to bi-sinusoidally distributed load on both top and bottom surfaces.
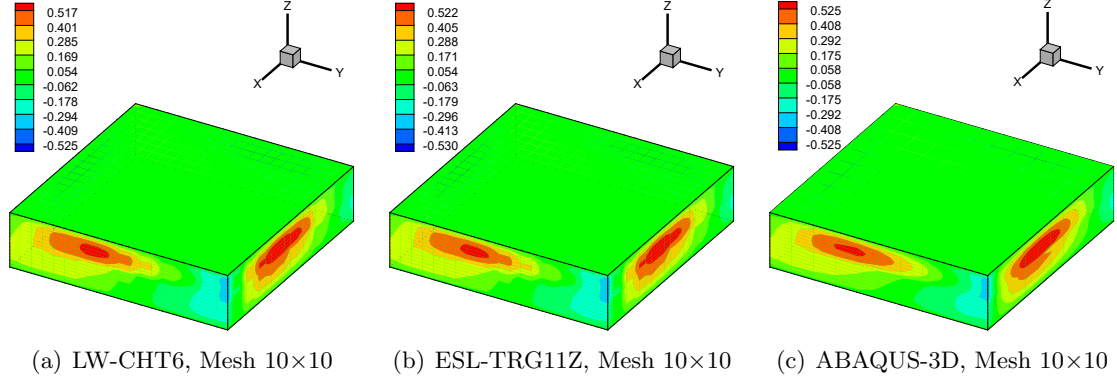
15

(a) LW-CHT6, Mesh 10×10   (b) ESL-TRG11Z, Mesh 10×10   (c) ABAQUS-3D, Mesh 10×10

Figure 7: Contour plot of σ_{yz}, thick simply supported plate ($a/h = 4$) with ($0°/30°$), $z \times 1$.

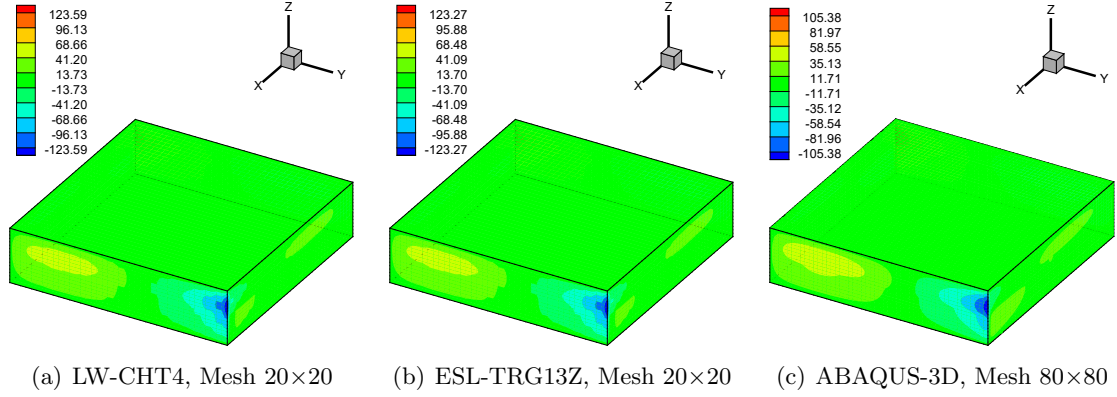(a) LW-CHT4, Mesh 20×20   (b) ESL-TRG13Z, Mesh 20×20   (c) ABAQUS-3D, Mesh 80×80

Figure 8: Contour plot of σ_{yz}, thin simply supported plate ($a/h = 50$) with ($0°/30°$), $z \times 12.5$.

5.3.3   Simply supported square thick and thin plates with ($-45°/45°$)

Based on the above two assessments, thick and thin simply supported square plates with lamination of ($-45°/45°$) are analyzed with CUF-based refined models adopting variable kinematics LW-CBTn and ESL-TRGnZ. Layers in each laminated plates have the same thickness $h/2$. The plates are imposed to uniformly distributed load p_0 on top surface, as shown in Eq. (32). Plates with various span-to-thickness ratios ($a/h = 4, 20, 100$) are analyzed.

$$p_t(x, y) = p_0 \tag{32}$$

Table 3 summarizes the results on the two-layered angle-ply thick, moderately thick and thin plates, in which the maximum relative error is 3%. It can be concluded that thin laminated plates tend to use more refined mesh to guarantee convergence. Since variable kinematics are adopted, the numbers of expansions used in the thickness functions can be decided by the level of accuracy required in specific situations. With a sufficient number of expansion, CUF-based refined models can provide converged numerically approximated solutions with requisite accuracy.

Fig. 9 shows the through-the-thickness variation of stresses. Note that when such simple supports are enforced on the four edges of a plate, σ_{xz} on point ($\frac{a}{2}, 0$) and σ_{yz} on point ($0, \frac{b}{2}$) are different from 0, which has also been shown by the former two numerical cases as in Figs. 4 to 6.

16
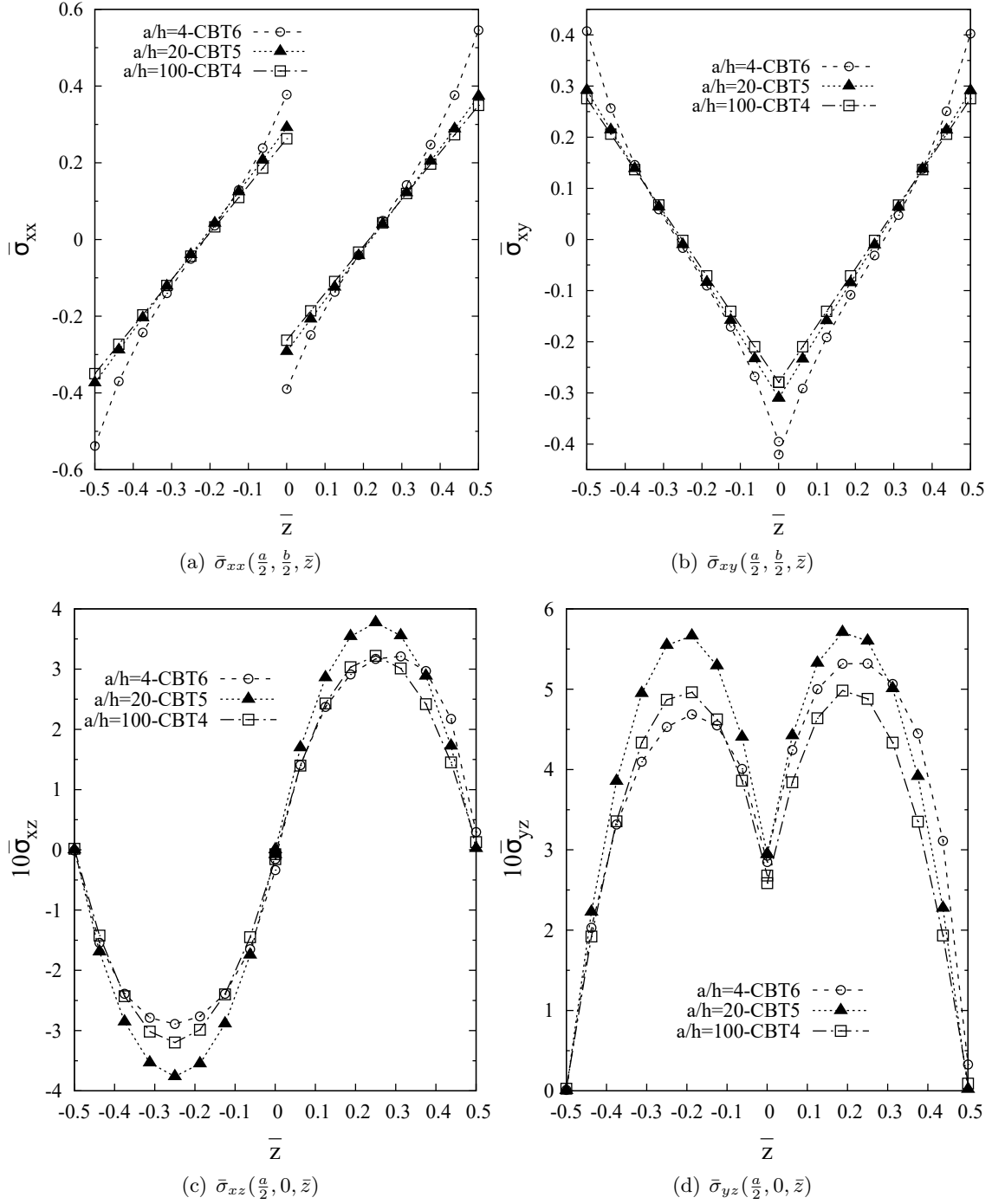
Figure 9: Through-the-thickness variation of stresses, $(-45°/45°)$ square plate imposed to uniformly distributed load on the top surface under simply supported boundary conditions.

17

Table 3: Displacement and stress evaluation of simply-supported square plates with $(-45°/45°)$ subjected to uniformly distributed load on top surface.

a/h	Kinematics	Mesh	$\bar{w}$ $(\frac{a}{2}, \frac{b}{2}, \frac{h}{2})$	$\bar{\sigma}_{xx}$ $(\frac{a}{2}, \frac{b}{2}, \frac{h}{2})$	$\bar{\sigma}_{yy}$ $(\frac{a}{2}, \frac{b}{2}, \frac{h}{2})$	$\bar{\sigma}_{xy}$ $(\frac{a}{2}, \frac{b}{2}, \frac{-h}{2})$	$10\bar{\sigma}_{xz}$ $(\frac{a}{2}, 0, \frac{h}{4})$	$10\bar{\sigma}_{yz}$ $(\frac{a}{2}, 0, \frac{h}{4})$	$\bar{\sigma}_{zz}$ $(\frac{a}{2}, \frac{b}{2}, \frac{h}{2})$	DOFs
	LW-CBT4	8×8	3.227	0.5423	0.5423	0.4046	3.262	5.400	0.9976	6069
	LW-CBT4	10×10	3.227	0.5453	0.5453	0.4073	3.269	5.431	1.000	9261
	LW-CBT5	10×10	3.229	0.5454	0.5454	0.4074	3.167	5.316	1.001	11907
4	LW-CBT6	10×10	3.229	0.5454	0.5454	0.4073	3.169	5.319	0.9988	14553
	ESL-TRG7Z	10×10	3.224	0.5443	0.5443	0.4066	3.333	5.472	0.9902	11907
	ESL-TRG9Z	10×10	3.228	0.5453	0.5453	0.4073	3.187	5.353	1.005	14553
	ESL-TRG11Z	10×10	3.228	0.5453	0.5453	0.4073	3.150	5.325	0.9951	17199
	LW-CBT3	10×10	1.245	0.3727	0.3727	0.2907	3.723	5.531	1.057	6615
	LW-CBT3	12×12	1.246	0.3737	0.3737	0.2916	3.789	5.620	1.059	9375
	LW-CBT4	12×12	1.246	0.3737	0.3737	0.2916	3.788	5.619	0.9975	13125
20	LW-CBT5	12×12	1.246	0.3737	0.3737	0.2916	3.771	5.600	0.9973	16875
	ESL-TRG7Z	12×12	1.245	0.3733	0.3733	0.2914	3.949	5.807	1.036	16875
	ESL-TRG9Z	12×12	1.246	0.3737	0.3737	0.2916	3.776	5.610	1.013	20625
	ESL-TRG11Z	12×12	1.246	0.3737	0.3737	0.2916	3.742	5.592	0.9947	24375
	LW-CBT3	14×14	1.056	0.3493	0.3493	0.2751	3.213	4.823	1.003	12615
	LW-CBT3	16×16	1.057	0.3496	0.3496	0.2754	3.225	4.883	1.031	16335
100	LW-CBT4	16×16	1.057	0.3496	0.3496	0.2754	3.221	4.880	1.000	22869
	ESL-TRG9Z	16×16	1.057	0.3495	0.3495	0.2753	2.763	3.773	1.196	35937
	ESL-TRG11Z	16×16	1.057	0.3496	0.3496	0.2754	3.195	4.982	1.034	42471

5.3.4 Simply supported square thick and thin plates with $(-45°/0°/90°/45°)$

In engineering application, thin-walled laminated structures usually have more general and complicated stacking sequence. In this section, numerical solutions for a four layered square plate with lamination $(-45°/0°/90°/45°)$ are proposed. The plates are subjected to bi-sinusoidally distributed load on the top surface (as described in Eq. (33)) under simply supported boundary conditions. Span-to-thickness ratios $a/h = 4, 50$ are considered.

$$p_t(x, y) = p_0 \sin \frac{\pi x}{a} \sin \frac{\pi y}{b} \tag{33}$$

The numerical results have been summarized in Table 4, and stress variation through thickness on two in-plane points are illustrated as shown in Fig. 10. It can be found that even if with a significant number of expansion ESL-TRGnZ have achieved the numerical convergence, the corresponding through-the-thickness variation of transverse shear stresses are still not continuous at layer interfaces, while this is not the case for the plate with two layers as shown in Fig. 4 and Fig. 6. This phenomenon can also be found in Fig. 5 (c) and (d). Compared with ESL-TRGnZ, LW-CHTn models are more suitable for laminates with more than two layers in capturing the zig-zag behaviors.

Fig. 11 presents the contour plots of σ_{xz} for both the thick and thin plates, which show that CUF-based advanced kinematics can capture very detailed stress field on laminated structures. Similar with Figs. 7 and 8, it can also be observed that the location of maximum stress moves from the edge center to edge corner when the laminated plate becomes thinner.

18

Table 4: Displacement and stress evaluation of simply supported square plate with $(-45°/0°/90°/45°)$, subjected to bi-sinusoidally distributed load on the top surface.

a/h	Kinematics	Mesh	$\bar{w}$ $(\frac{a}{2}, \frac{b}{2}, \frac{h}{2})$	$\bar{\sigma}_{xx}$ $(\frac{a}{2}, \frac{b}{2}, \frac{h}{2})$	$\bar{\sigma}_{yy}$ $(\frac{a}{2}, \frac{b}{2}, \frac{h}{2})$	$\bar{\sigma}_{xy}$ $(\frac{a}{2}, \frac{b}{2}, \frac{-h}{2})$	$10\bar{\sigma}_{xz}$ $(\frac{a}{2}, 0, \frac{3h}{8})$	$10\bar{\sigma}_{yz}$ $(\frac{a}{2}, 0, \frac{h}{8})$	$\bar{\sigma}_{zz}$ $(\frac{a}{2}, \frac{b}{2}, \frac{h}{2})$	DOFs
4	LW-CBT3	6×6	2.517	0.3913	0.3834	0.2421	1.259	3.060	1.016	4563
	LW-CBT3	8×8	2.518	0.3935	0.3856	0.2453	1.263	3.057	1.014	7803
	LW-CBT4	8×8	2.518	0.3933	0.3854	0.2453	1.266	3.058	1.001	11271
	ESL-TRG9Z	8×8	2.508	0.3925	0.3841	0.2445	1.154	3.010	1.004	9537
	ESL-TRG11Z	8×8	2.510	0.3924	0.3842	0.2445	1.148	3.060	1.003	11271
50	LW-CBT3	14×14	0.6846	0.1791	0.1650	0.1159	0.4639	3.485	1.016	22707
	LW-CBT3	16×16	0.6852	0.1793	0.1651	0.1161	0.4537	3.559	1.012	29403
	LW-CBT4	16×16	0.6852	0.1792	0.1651	0.1161	0.4552	3.558	1.000	42471
	ESL-TRG9Z	16×16	0.6847	0.1792	0.1650	0.1160	0.4426	3.721	0.6130	35937
	ESL-TRG11Z	16×16	0.6847	0.1793	0.1651	0.1160	0.3534	3.572	1.651	42471
	ESL-TRG13Z	16×16	0.6848	0.1792	0.1650	0.1160	0.4473	3.595	0.5273	49005
	ESL-TRG15Z	16×16	0.6849	0.1792	0.1651	0.1160	0.5329	3.589	1.095	55539
	ESL-TRG17Z	16×16	0.6849	0.1792	0.1651	0.1160	0.4852	3.590	1.065	62073

(a) $\bar{\sigma}_{xx}(\frac{a}{2}, \frac{b}{2}, \bar{z})$

(b) $\bar{\sigma}_{xy}(\frac{a}{2}, \frac{b}{2}, \bar{z})$

(c) $\bar{\sigma}_{xz}(\frac{a}{2}, 0, \bar{z})$

(d) $\bar{\sigma}_{yz}(\frac{a}{2}, 0, \bar{z})$

19

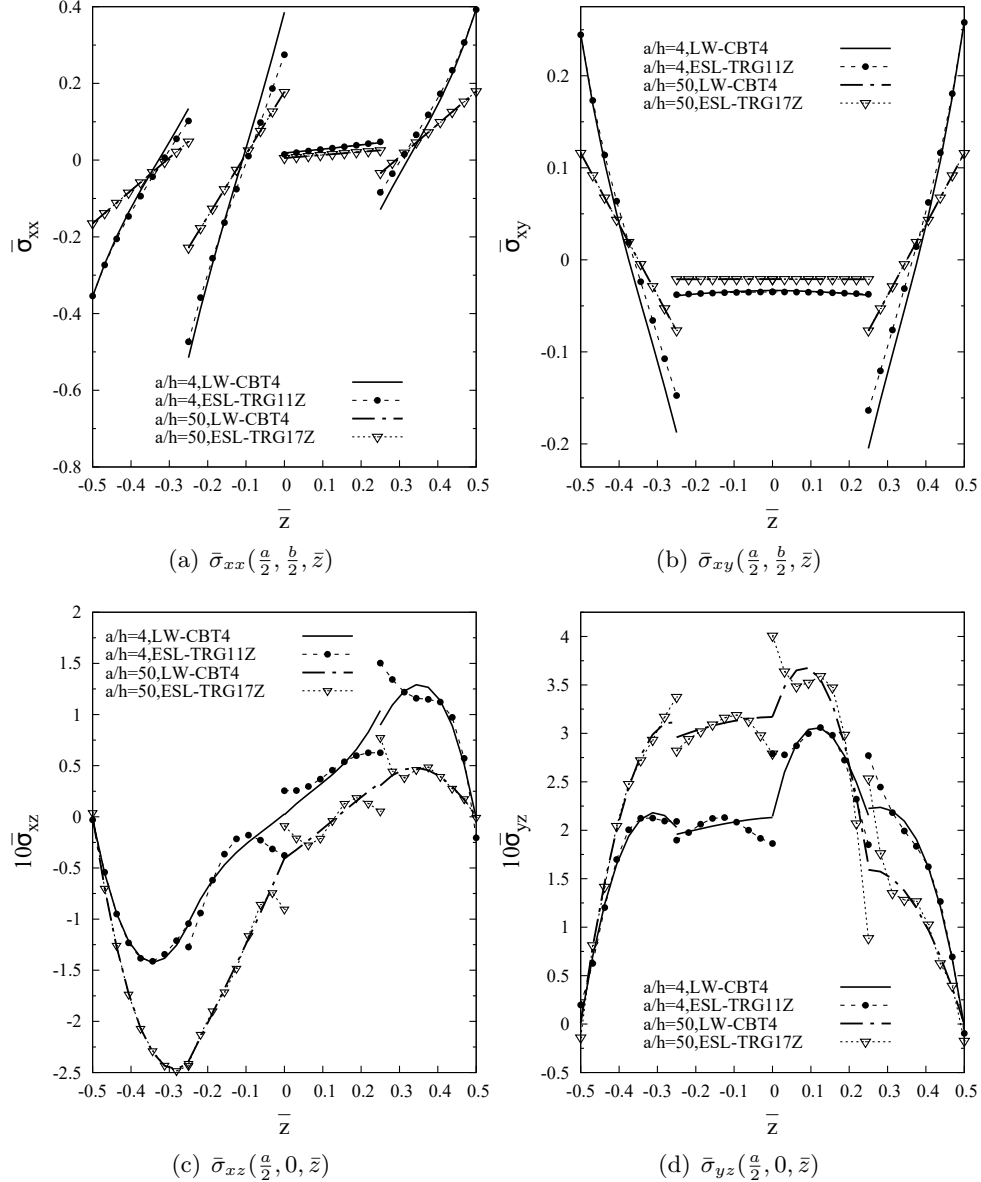Figure 10: Through-the-thickness variation of stresses, simply supported plate with $(-45°/0°/90°/45°)$ under bi-sinusoidally distributed load on the top surface.

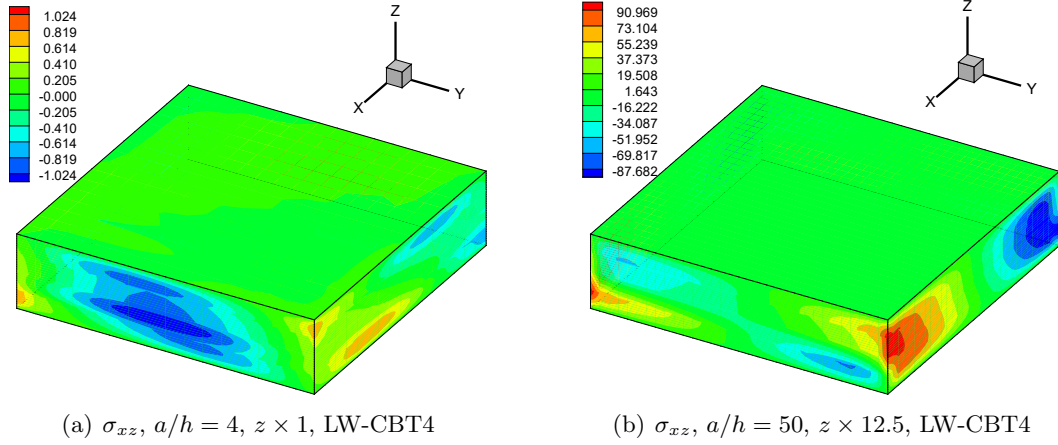(a) σ_{xz}, $a/h = 4$, $z \times 1$, LW-CBT4   (b) σ_{xz}, $a/h = 50$, $z \times 12.5$, LW-CBT4

Figure 11: σ_{xz} contour plot of $(-45°/0°/90°/45)$ plate loaded to bi-sinusoidally distributed load on the top surface under simply-supported boundary conditions.

5.3.5   Square plate with $(0°/60°)$ subjected to mixed clamped-free boundary conditions

Square plates with stacking sequence $(0°/60°)$ under uniformly distributed load p_0 on top surface according to Eq. (32) are considered. The two layers have equal thickness $h/2$. Span-to-thickness ratios considered are $a/h = 10$ and 50. The mixed clamped-free boundary conditions adopted are denoted as CFCC, to be specific: clamped on edge $x = 0$, free on edge $y = 0$, clamped on edge $x = a$, clamped on edge $y = b$.

Displacement and stresses results have been summarized in Table 5. Even if variable kinematics ESL-TRGnZ achieved numerically converged results, they still consume more computation resources than LW-CBTn models, given that only two layers exist in the laminated plate. Fig. 12 reports the stress variation through the thickness of the plate, in which $\bar{\sigma}_{yz}$ in Fig. 12 (d) is in good agreement with the results proposed by Nik [21].

Table 5: Displacement and stress evaluation of square plate with $(0°/60)$ subjected to uniformly distributed load on the top surface under mixed boundary conditions CFCC.

a/h	Kinematics	Mesh	$\bar{w}$ $(\frac{a}{2}, \frac{b}{2}, \frac{h}{2})$	$\bar{\sigma}_{xx}$ $(\frac{a}{2}, \frac{b}{2}, \frac{-h}{2})$	$\bar{\sigma}_{yy}$ $(\frac{a}{2}, \frac{b}{2}, \frac{h}{2})$	$\bar{\sigma}_{xy}$ $(\frac{a}{4}, \frac{b}{4}, \frac{h}{2})$	$\bar{\sigma}_{xz}$ $(\frac{a}{4}, \frac{b}{4}, \frac{-h}{4})$	$\bar{\sigma}_{yz}$ $(\frac{a}{2}, \frac{b}{4}, \frac{h}{4})$	$\bar{\sigma}_{zz}$ $(\frac{a}{2}, \frac{b}{2}, \frac{h}{2})$	DOFs
	LW-CBT3	8×8	0.7987	-0.5601	0.2196	0.09479	0.5288	0.08173	0.5250	4335
	LW-CBT3	12×12	0.7992	-0.5521	0.2156	0.08228	0.5204	0.08187	0.5311	9375
	LW-CBT4	12×12	0.7994	-0.5518	0.2155	0.08424	0.5202	0.08219	0.5001	13125
10	LW-CBT5	12×12	0.7996	-0.5517	0.2157	0.08774	0.5194	0.08067	0.5007	16875
	ESL-TRG9Z	12×12	0.7995	-0.5517	0.2156	0.08923	0.5239	0.08221	0.5066	20625
	ESL-TRG11Z	12×12	0.7996	-0.5516	0.2157	0.09352	0.5185	0.08089	0.4975	24375
	ESL-TRG13Z	12×12	0.7997	-0.5517	0.2154	0.09528	0.5156	0.07977	0.4934	28125
	LW-CBT3	16×16	0.4982	-0.5333	0.2021	0.05675	0.5322	0.09120	0.5345	16335
	LW-CBT3	20×20	0.4984	-0.5321	0.2017	0.05510	0.5292	0.09111	0.5285	25215
	LW-CBT4	20×20	0.4984	-0.5320	0.2018	0.05589	0.5295	0.09101	0.5022	35301
50	LW-CBT5	20×20	0.4984	-0.5320	0.2018	0.05649	0.5290	0.09032	0.4970	45387
	ESL-TRG9Z	20×20	0.4984	-0.5321	0.2017	0.05510	0.5292	0.09111	0.5285	55473
	ESL-TRG11Z	20×20	0.4984	-0.5320	0.2015	0.05693	0.5297	0.08992	0.4978	65559

(a) $\bar{\sigma}_{xx}\left(\frac{a}{2}, \frac{b}{2}, \bar{z}\right)$

(b) $\bar{\sigma}_{xy}\left(\frac{a}{4}, \frac{b}{4}, \bar{z}\right)$

(c) $\bar{\sigma}_{xz}\left(\frac{a}{4}, \frac{b}{4}, \bar{z}\right)$

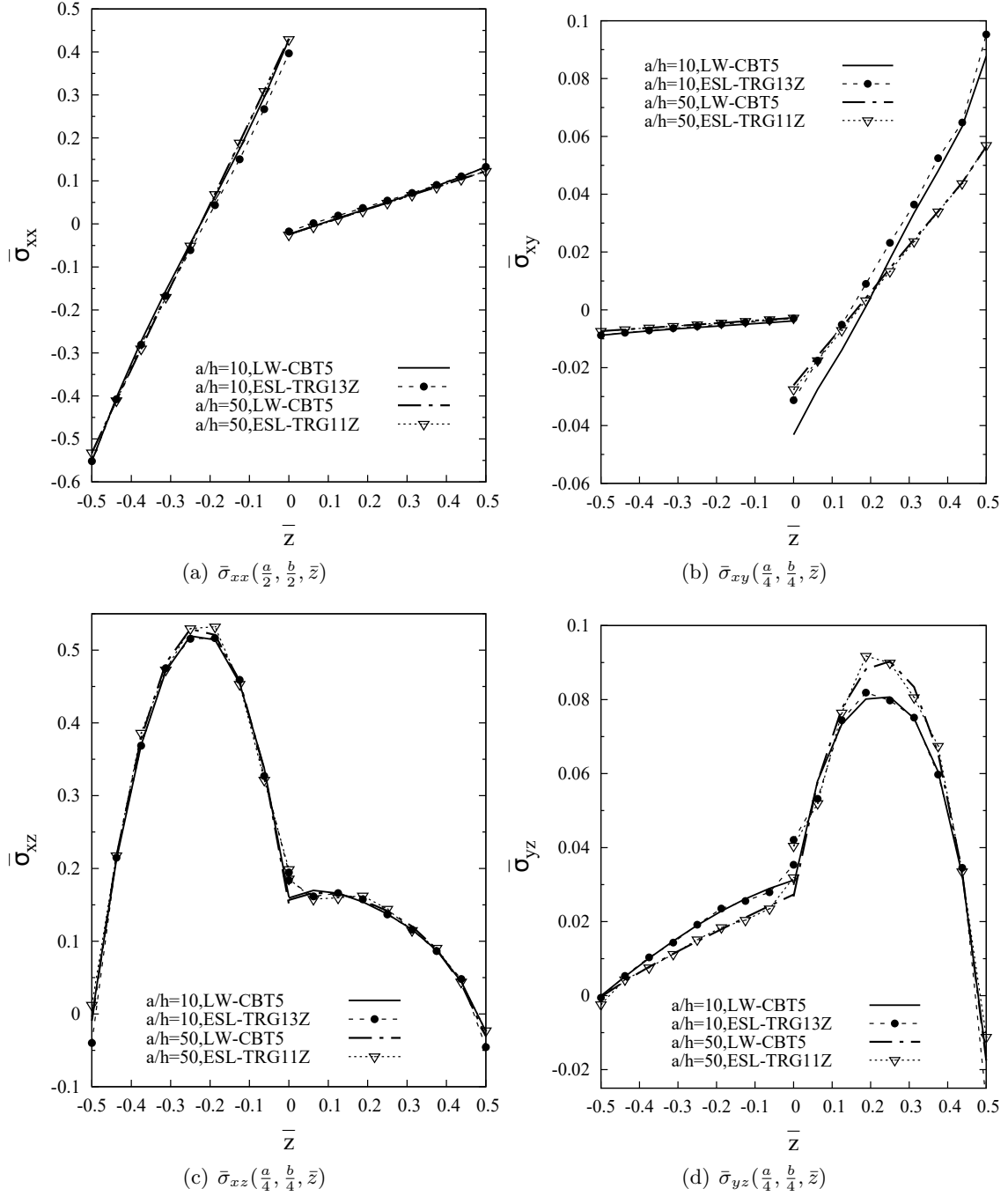(d) $\bar{\sigma}_{yz}\left(\frac{a}{4}, \frac{b}{4}, \bar{z}\right)$

Figure 12: Through-the-thickness variation of stresses, $(0°/60°)$ plate with $a/h = 10$ and 50, subjected to uniformly distributed load on the top surface under mixed boundary conditions CFCC.

6 Conclusions

This work studied angle-ply laminated plates with CUF-based variable kinematic LW models adopting Chebyshev polynomials of the first kind (LW-CBTn) and ESL models based on full trigonometric series expansion (ESL-TRGnZ). Simply supported and mixed clamped-free boundaries that are suitable for displacement-based 3D models, 2D LW models and ESL models with non-Taylor series are adopted for analysis. Based on the numerical study, the following conclusions have been drawn:

1. CUF provides a unified approach to integrate a variety of approximation theories (including both interpolation polynomials and series expansion theories) to obtain refined FE model.

2. With CUF-based variable kinematics, it is convenient to increase the numbers of expansions adopted in the thickness function to achieve numerical convergence with requisite accuracy.

3. In the cases with simply supported boundary conditions, by using clearly stated geometrical edge supports as defined in Table 1, the results for angle-ply laminated plate obtained with displacement-based refined plate models are verified by comparison with ABAQUS 3D solutions.

4. Both the two classes of variable kinematics adopted (LW-CBTn and ESL-TRGnZ) can achieve numerical convergence, yet ESL-TRGnZ models tend to use more expansions in the thickness functions in the whole through-the-thickness domain.

5. For angle-ply laminated plates with a large number of layers, compared with LW models (LW-CBTn), ESL models with Murakami's zig-zag function (ESL-TRGnZ) are less efficient in obtaining continuous transverse shear stresses through the thickness even if a significant number of expansion terms are adopted in some cases.

6. CUF-based refined 2D FE models can capture 3D stress field in detail with much fewer computation costs compared with 3D FE models while guaranteeing accuracy.

7. Some numerical results on angle-ply laminated plates are reported, which can be used as the reference for future study.

In the above discussed numerical cases, ESL models adopting full trigonometric series (ESL-TRGnZ) have been proved to be less numerically efficient compared with LW models (LW-CTBn). Since Fourier Transform have been successfully applied in signal processing, the application of trigonometric series in the analysis of piezoelectric components might be worth of the efforts. The above work can also be extended to the formulations of shells in the future.

References

[1] W. Koiter, On the foundations of the linear theory of thin elastic shell, Proc Kon Nederl Akad Wetensch 73 (3) (1970) 169–195.

[2] P. Naghdi, The theory of plates and shells, Handbuch der Physik, vol. VI a-2 (1972) 425–640.

[3] J. N. Reddy, A simple higher-order theory for laminated composite plates, Journal of Applied Mechanics 51 (4) (1984) 745–752.

[4] J. N. Reddy, Mechanics of laminated composite plates and shells: theory and analysis, CRC Press, 2004.

[5] A. N. Palazotto, Nonlinear analysis of shell structures, AIAA Series, 1992.

[6] N. J. Pagano, Exact solutions for rectangular bidirectional composites and sandwich plates, Journal of Composite Materials 4 (1) (1970) 20–34.

[7] N. Pagano, H. J. Hatfield, Elastic behavior of multilayered bidirectional composites, AIAA Journal 10 (7) (1972) 931–933.

[8] S. Srinivas, A. Rao, A three-dimensional solution for plates and laminates, Journal of the Franklin Institute 291 (6) (1971) 469–481.

[9] J. Ren, Bending of simply-supported, antisymmetrically laminated rectangular plate under transverse loading, Composites Science and Technology 28 (3) (1987) 231–243.

[10] A. K. Noor, W. S. Burton, Three-dimensional solutions for antisymmetrically laminated anisotropic plates, Journal of Applied Mechanics 57 (1) (1990) 182–188.

[11] M. Savoia, J. Reddy, A variational approach to three-dimensional elasticity solutions of laminated composite plates, Journal of Applied Mechanics 59 (2S) (1992) S166–S175.

[12] V. Carvelli, M. Savoia, Assessment of plate theories for multilayered angle-ply plates, Composite Structures 39 (3) (1997) 197–207.

[13] G. Kulikov, S. Plotnikova, Exact 3D stress analysis of laminated composite plates by sampling surfaces method, Composite Structures 94 (12) (2012) 3654–3663.

[14] G. Kulikov, S. Plotnikova, Three-dimensional exact analysis of piezoelectric laminated plates via a sampling surfaces method, International Journal of Solids and Structures 50 (11) (2013) 1916–1929.

[15] R. A. Chaudhuri, K. R. Abu-Arja, Static analysis of moderately-thick finite antisymmetric angle-ply cylindrical panels and shells, International Journal of Solids and Structures 28 (1) (1991) 1–15.

[16] J. He, Z. Zhang, Bending analysis of antisymmetric angle-ply laminated plates including transverse shear effects, Composite Structures 34 (4) (1996) 437–444.

[17] J. He, A refined shear deformation theory of laminated plates and shells, in: Proceedings of the Seventh International Conference on Composite Materials, Vol. 4, 1989, pp. 180–182.

[18] V. Piskunov, V. Verijenko, S. Adali, P. Tabakov, V. Prisyazhnyouk, S. Buryhin, Rational transverse shear deformation higher-order theory of anisotropic laminated plates and shells, International Journal of Solids and Structures 38 (36) (2001) 6491–6523.

[19] M. Ray, Zeroth-order shear deformation theory for laminated composite plates, Journal of Applied Mechanics 70 (3) (2003) 374–380.

[20] H. Zuo, Z. Yang, X. Chen, Y. Xie, H. Miao, Analysis of laminated composite plates using wavelet finite element method and higher-order plate theory, Composite Structures (131) (2015) 248–258.

[21] A. M. N. Nik, M. Tahani, Analytical solutions for bending analysis of rectangular laminated plates with arbitrary lamination and boundary conditions, Journal of Mechanical Science and Technology 23 (8) (2009) 2253–2267.

[22] J. M. Whitney, A. W. Leissa, Analysis of heterogeneous anisotropic plates, Journal of Applied Mechanics 36 (2) (1969) 261–266.

[23] J. Whitney, Bending-extensional coupling in laminated plates under transverse loading, Journal of Composite Materials 3 (1) (1969) 20–28.

[24] A. Loredo, Exact 3D solution for static and damped harmonic response of simply supported general laminates, Composite Structures 108 (2014) 625–634.

[25] M. Özakça, E. Hinton, N. Rao, Comparison of three-dimensional solid elements in the analysis of plates, Computers & Structures 42 (6) (1992) 953–968.

[26] A. Bogdanovich, A. Birger, Three-dimensional stress field analysis in uniformly loaded, simply supported composite plates, Computers & Structures 52 (2) (1994) 237–257.

[27] P. Kumari, S. Kapuria, Boundary layer effects in rectangular cross-ply Levy-type plates using zigzag theory, ZAMM-Journal of Applied Mathematics and Mechanics/Zeitschrift für Angewandte Mathematik und Mechanik 91 (7) (2011) 565–580.

[28] S. Kapuria, P. Kumari, Boundary layer effects in Levy-type rectangular piezoelectric composite plates using a coupled efficient layerwise theory, European Journal of Mechanics-A/Solids 36 (2012) 122–140.

[29] F. Tornabene, E. Viola, Static analysis of functionally graded doubly-curved shells and panels of revolution, Meccanica 48 (4) (2013) 901–930.

[30] T. Kant, B. Manjunatha, On accurate estimation of transverse stresses in multilayer laminates, Computers & Structures 50 (3) (1994) 351–365.

[31] Y. Desai, G. Ramtekkar, A. Shah, A novel 3D mixed finite-element model for statics of angle-ply laminates, International Journal for Numerical Methods in Engineering 57 (12) (2003) 1695–1716.

[32] C. Chinosi, L. Della Croce, M. Cinefra, E. Carrera, Approximation of anisotropic multilayered plates through RMVT and MITC elements, Composite Structures 158 (2016) 252–261.

[33] E. Carrera, Theories and finite elements for multilayered, anisotropic, composite plates and shells, Archives of Computational Methods in Engineering 9 (2) (2002) 87–140.

[34] E. Carrera, Theories and finite elements for multilayered plates and shells: a unified compact formulation with numerical assessment and benchmarking, Archives of Computational Methods in Engineering 10 (3) (2003) 215–296.

[35] E. Carrera, M. Cinefra, M. Petrolo, E. Zappino, Finite element analysis of structures through unified formulation, John Wiley & Sons, 2014.

[36] C. Chinosi, L. Della Croce, Mixed-interpolated elements for thin shells, Communications in Numerical Methods in Engineering 14 (12) (1998) 1155–1170.

[37] K. J. Bathe, P. S. Lee, J. F. Hiller, Towards improving the MITC9 shell element, Computers & Structures 81 (8) (2003) 477–489.

[38] M. Cinefra, S. Valvano, A variable kinematic doubly-curved MITC9 shell element for the analysis of laminated composites, Mechanics of Advanced Materials and Structures 23 (11) (2016) 1312–1325.

[39] M. Filippi, M. Petrolo, S. Valvano, E. Carrera, Analysis of laminated composites and sandwich structures by trigonometric, exponential and miscellaneous polynomials and a MITC9 plate element, Composite Structures 150 (2016) 103–114.

[40] E. Carrera, M. Cinefra, G. Li, G. Kulikov, MITC9 shell finite elements with miscellaneous through-the-thickness functions for the analysis of laminated structures, Composite Structures 154 (2016) 360–373.

[41] E. Carrera, M. Filippi, E. Zappino, Laminated beam analysis by polynomial, trigonometric, exponential and zig-zag theories, European Journal of Mechanics-A/Solids 41 (2013) 58–69.

[42] M. Filippi, A. Pagani, M. Petrolo, G. Colonna, E. Carrera, Static and free vibration analysis of laminated beams by refined theory based on Chebyshev polynomials, Composite Structures 132 (2015) 1248–1259.

[43] E. Carrera, G. Giunta, Hierarchical evaluation of failure parameters in composite plates, AIAA Journal 47 (3) (2009) 692–702.

[44] A. Pagani, A. de Miguel, M. Petrolo, E. Carrera, Analysis of laminated beams via Unified Formulation and Legendre polynomial expansions, Composite Structures 156 (2016) 78 – 92, 70th Anniversary of Professor J. N. Reddy.

[45] H. Murakami, Laminated composite plate theory with improved in-plane responses, Journal of Applied Mechanics 53 (3) (1986) 661–666.

[46] R. M. Jones, Mechanics of Composite Materials, CRC Press, 1998.